Refractivity Influence on DSS Doppler Data

F. B. Winn
Tracking and Orbit Determination Section
R. K. Leavitt
Flight Operations and DSN Programming Section

Doppler data from deep space missions show terrestrial media contamination influences even after least-square fitting. Cross-correlation between solution parameters and the media-induced errors is large enough to adversely affect parameter least-square adjustments. When a scale factor for Cain's tropospheric refractivity profile is included in the parameter list, the media-induced observed-minus-computed (O − C) structures do not appear above 15-deg elevation. When the scale factor is not included, O − C structures commence to appear at ~25-deg elevation.

I. Introduction

Hamilton and Melbourne (Ref. 1) have shown that low-elevation doppler data, from 0- to 15-deg elevation, can essentially double the information extractable from a single pass of doppler data. Thus, the theoretical value of ultra-low-elevation doppler observations for deep space probe navigation is recognized.

II. Evidence of Terrestrial Media Contamination

Low-elevation observations of extraterrestrial objects are subject to terrestrial media contamination; and indeed, the O − C residuals[1] (after the fit[2]) of *Lunar Orbiter IV*,[3] *Mariner VI*,[4] and *Surveyor VII*[5] exhibit elevation-dependent signatures or structures (Fig. 1). Figure 1 reveals the similarities of the different O − C residuals sets in as far as low-elevation, unmodeled influences are concerned.

[1]Observed-minus-computed residuals (coherent two-way doppler data: CC3).

[2]Recursive least-square fitting to doppler data accomplished by the use of JPL's double-precision orbit determination program (DPODP) (Ref. 2).

[3]*Lunar Orbiter IV* analyses by W. L. Sjogren.

[4]*Mariner VI* analyses by J. W. Zielenbach.

[5]*Surveyor VII* analyses by F. B. Winn.

The high-frequency data noise of the *Lunar Orbiters* masks the finer structure of the residuals; however, even with the limited resolution of the *Lunar Orbiter* data, the elevation dependence of the O − C variation is clear. The *Mariner* and *Surveyor* O − C residuals do not suffer for resolution and they show the "diurnal" signature quite well.

The atmospheric influences, responsible for the O − C variations of Fig. 1, can be attributed to two principal sources: ionosphere and troposphere. The ionosphere is not a specific part of this study although ionospheric charged particle calibrations of the data involved in this study are currently underway and are expected to bring about an improvement of the results.

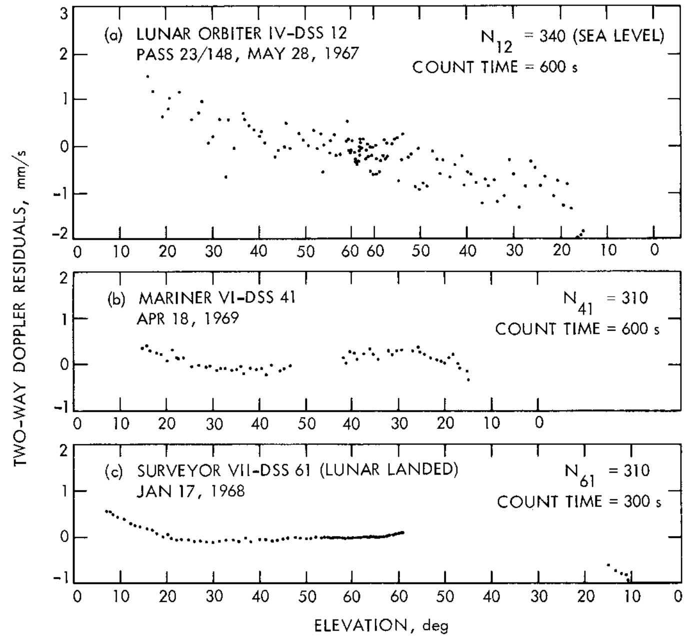

Fig. 1. Two-way doppler residuals as a function of elevation

III. Modelling

Many model atmospheres assume that refractivity decreases exponentially with height above sea level. Formulated, this concept appears as

$$N = N_0 \exp(-Bh) \tag{1}$$

where

h = height above sea level

N = refractivity at height h

N_0 = refractivity at sea level

B = inverse scale height

The specific model atmosphere which formed the basis of the JPL SPODP[6] and DPODP (Ref. 4) tropospheric model is

$$N = 340 \exp(-0.142\, h) \tag{2}$$

Equation (2) was utilized[7] to compute a set of tabular range corrections as a function of elevation. The tabular arguments were then fitted by the empirical function

$$\Delta\rho_r = C_1 \left(\frac{N}{340}\right) [\sin(\gamma) + C_2]^{C_3} \tag{3}$$

where

$\Delta\rho_r$ = range correction due to group velocity retardation, km

γ = geometric elevation angle

N = refractivity scaler (340 is the sea level scaler)

and the constants C_1, C_2, C_3 were determined to be

$$C_1 = 1.8958 \times 10^{-3}$$

$$C_2 = 6.483 \times 10^{-2}$$

$$C_3 = -1.4$$

The influence of the troposphere upon the doppler, $\Delta\dot{\rho}_r$, was computed from differenced range corrections normalized per second of time:

$$\Delta\dot{\rho}_r = \frac{\left[\Delta\rho_r\left(\gamma + \frac{\dot{\gamma}\,\tau_c}{2}\right) - \Delta\rho_r\left(\gamma - \frac{\dot{\gamma}\,\tau_c}{2}\right)\right]}{\tau_c} \tag{4}$$

where

$\dot{\gamma}$ = time rate of change of γ, γ units/s

τ_c = doppler count time, s

[6]SPODP = single-precision orbit determination program (Ref. 3).
[7]By D. L. Cain, JPL Tracking and Orbit Determination Section.

In terms of Eq. (3) variables,

$$\Delta\dot{\rho}_r = \left(\frac{C_1}{\tau_c}\right)\left(\frac{N}{340}\right)\left\{\left[\sin\left(\gamma + \frac{\dot{\gamma}\tau_c}{2}\right) + C^2\right]^{C_3} - \left[\sin\left(\gamma - \frac{\dot{\gamma}\tau_c}{2}\right) + C_2\right]^{C_3}\right\} \tag{5}$$

Equations (3) and (5) constitute the SPODP and DPODP (5.1 versions or earlier) refraction models.

Liu (Ref. 4) scaled Eqs. (3) and (5) in accordance with the findings of a study conducted by Smyth Research Associates. The refractivity scalers were determined to be

$$N_{11}\,(\text{Goldstone}) = 240$$
$$N_{42}\,(\text{Canberra}) = 310$$
$$N_{61}\,(\text{Madrid}) = 300$$

where the subscripts indicate the DSS. If the assumptions behind Eq. (5) are valid, then rescaling of the function can be accomplished by empirically fitting spacecraft tracking data.

Due to the abundance and employment of low-elevation data (below 15 deg) in *Surveyor* mission analysis (Refs. 5–7), coupled with low data noise ($\sigma_{CC3} \simeq$ 0.06 mm/s for a 300-s count time) and the fact that the *Surveyor* data were acquired over large declination ranges, makes *Surveyor* data quite useful in a refractivity study. The abundance of low-elevation data is essential in that the partial of the doppler observable (CC3) with respect to the refractivity scaler N becomes exponentially increasing at low elevation, increasing an order of magnitude from 20 deg down to 5 deg. The large declination sweeps that the *Surveyors* underwent during a lunar day tend to modify the $\partial CC3/\partial N$ profile from pass to pass, thus varying parameter cross-correlations from pass to pass.

The observed fact that the partial of the observable (two-way doppler) with respect to N is unique in signature, particularly at low elevations, when compared to the signature of the partials of the observable with respect to the remaining parameter list (Table 1), demonstrates the separability of N statistically from the other solution parameters (Figs. 2, 3, and 4).

Correlation matrices (Table 2) similarly show the doppler observable sensitivities to the tropospheric refraction parameter N to be unique. The cross-correlations are of sufficient size, however, to indicate that if the tropospheric refraction scaler is variable and not treated as such, or not solved for, the remaining parameter list will be adversely influenced.

Table 1. Parameter list

Parameter	Definition
R	selenocentric distance of a *Surveyor*
LA	selenographic latitude of a *Surveyor*
LO	selenographic longitude of a *Surveyor*
r_{s_i}	spin-axis distance of DSS$_i$
LO_i	geocentric longitude of DSS$_i$
$\Delta a/a$	semi-major axis of the lunar orbit[a]
Δe	eccentricity of the lunar orbit[a]
$\Delta L + \Delta r$	mean lunar longitude[a]
Δp	rotation around the perigee axis of the lunar orbit[a]
Δq	rotation around the axis normal to the perigee axis in the plane of the orbit[a]
$e\Delta r$	rotation around the out-of-plane axis completing a right-handed system[a]

[a]Constitutes set III, two-body osculating elements (Ref. 8).

Table 2. 2 × 2 cross-correlations[a] of parameter list with respect to N_{42}

Parameter	Surveyor				
	I	III	V	VI	VII
R	−0.207	−0.087	−0.094	−0.001	0.178
LA	0.352	−0.097	−0.147	−0.009	−0.318
LO	0.191	0.069	0.219	0.016	0.349
$r_{s_{42}}$	0.664[b]	0.727[b]	0.777[b]	0.795[b]	0.724[b]
LO_{42}	0.187[b]	0.207[b]	0.404[b]	0.510[b]	0.315[b]
$\Delta a/a$	−0.187	0.161	−0.433	0.527	0.332
Δe	0.540	0.390	0.403	0.444	−0.490
$\Delta L + \Delta r$	−0.187	−0.167	0.455	−0.590	−0.335
Δp	0.505	0.484	0.517	0.451	0.379
Δq	0.235	0.002	0.330	0.099	0.132
$e\Delta r$	0.506	−0.498	−0.254	−0.362	0.154

[a]2 × 2 cross-correlations are derived from the normal equation matrix, and thus express the statistical separability of each parameter with respect to N independent of the other parameters of the list.

[b]DSS 42 spin-axis distances and longitudes were included because DSS 42 is the only station which tracked all *Surveyors*. This is based on all data collected by DSS 42 during the first lunar day of each *Surveyor* mission.

In a series of SPODP fits to *Surveyor VII* first-lunar-day tracking data, the "nominal values" of the refractivity scalers for DSSs 11, 42, and 61 were changed with the intent of "brute forcing" the weighted sum of the squares

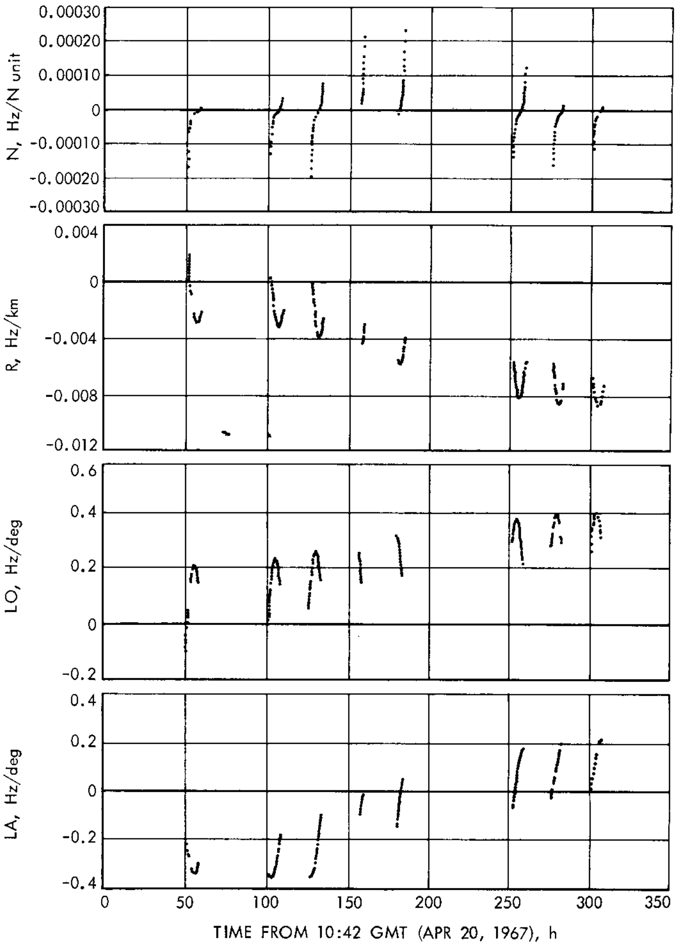

Fig. 2. Partials of *Surveyor III* two-way doppler with respect to *N*, *R*, *LO*, and *LA*

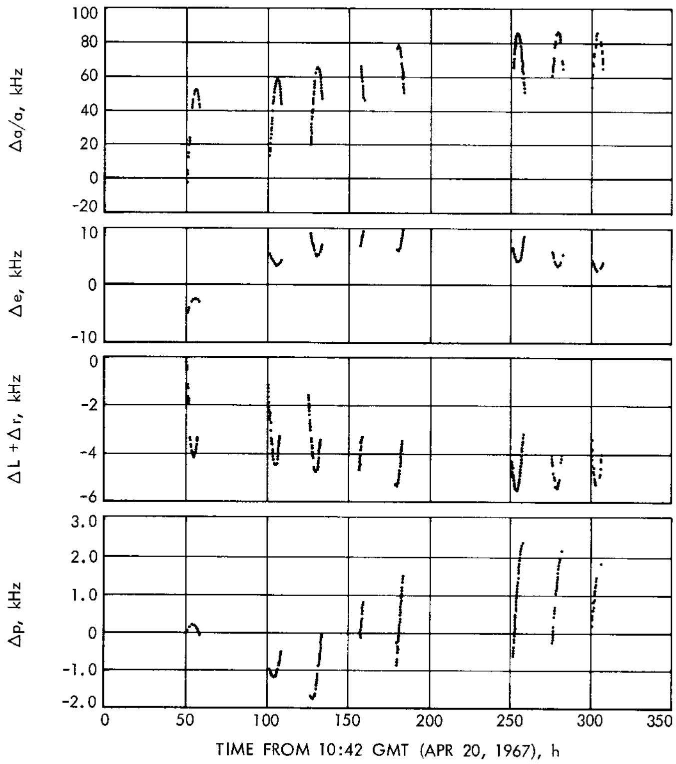

Fig. 3. Partials of *Surveyor III* two-way doppler with respect to $\Delta a/a$, Δe, $\Delta L + \Delta r$, and Δp

to a new "minimum."[8] The solutions are presented in Table 3, and the response of the spin-axis distance solutions of each DSS to the assigned N values is graphed in Fig. 5.

Once a minimum sum of the squares was achieved as a function of N for each DSS, it was noted that the "mean-best-fit" N for the lunation overcorrected some and undercorrected some of the passes (Ref. 7), that is, the O − C residuals still exhibited N-dependent or elevation-dependent signatures (Fig. 6) for some passes. The mean lunar day refractivity scaling factor is not optimum for the individual passes.

Three series of DPODP pass-by-pass fits were made to *Surveyor I, III, V, VI,* and *VII* tracking data sets (only those solutions associated with DSS 11 are presented at this time): the first series of fits solved for N, r_s, λ (DSS refractivity scalers, distance off the spin axis, and longitudes, respectively); the second series of reductions solved for N, r_s, and λ, but N was constrained by an *a priori* σ equal to 2% of the nominal value of N; and, finally, the third series solved for N solely.

[8]The data is off-weighted as a function of elevation; the weighting function is discussed later.

Table 3. Solution parameter sensitivities to *N*

N_{11}	0	240	240	340
N_{42}	0	280	310	340
N_{61}	0	270	300	340
$r_{s_{11}}$	5206.220	5206.209	5206.209	5206.204
LO_{11}	243.15090	243.15112	243.15112	243.15112
$r_{s_{42}}$	5205.335	5205.311	5205.308	5205.305
LO_{42}	148.98166	148.98192	148.98192	148.98192
$r_{s_{61}}$	4862.527	4862.515	4862.514	4862.512
LO_{61}	355.75143	355.75162	355.75161	355.75161
R	1739.302	1741.486	1741.582	1741.687
LA	−40.926	−40.863	−40.856	−40.859
LO	348.512	348.482	348.472	348.473

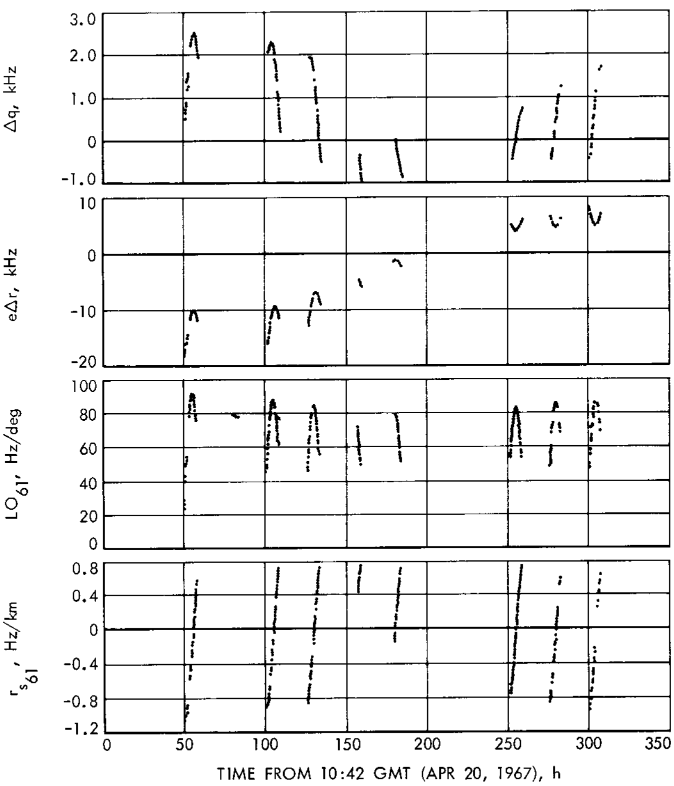

Fig. 4. Partials of *Surveyor III* two-way doppler with respect to Δq, $e\Delta r$, LO_{61}, and $r_{s_{61}}$

IV. Simultaneous Solutions for N_{11}, $r_{s_{11}}$, λ_{11}

In those solutions in which the *a priori* σ for N_{11}, $r_{s_{11}}$, and λ_{11} were set to 100 N units, 50 m, and 50 m, respectively, and a unit σ of 0.1 mm/s was applied to all doppler observations, the parameter cross-correlations became the single dominant trait of the fits. That is, the parameter cross-correlations and the variations of the cross-correlations generate a scatter in the parameter solutions (Fig. 7). The variation of the cross-correlations stems from data acquisition patterns and the changing pass-profile of the partial of the doppler observable with respect to the refraction parameter N_{11} (Fig. 8). Thus, it is apparent that r_s and N cannot be simultaneously solved for via a least-square adjustment of doppler data.

V. Data Fits to N_{11}, $r_{s_{11}}$, λ_{11} With N_{11} Subjected to *A Priori* Constraint

To diminish the parameter cross-correlation influences responsible for the solution parameter scatter, in the second series of DPODP fits, N_{11} was constrained by an *a priori* σ of 4 N units, that is, the *a priori* σ of N_{11} presumes that

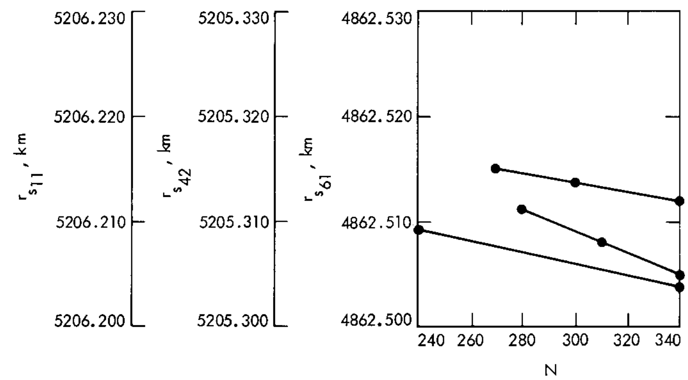

Fig. 5. DSS r_s solution sensitivity to N

true N_{11} must be within 2% of the nominal value 67% of the time. The assumption is fairly consistent with the radiosonde findings. The radiosonde analysis (Ref. 9) shows the maximum range of the tropospheric doppler error (peak to peak) at 5- to 10-deg elevation to be $\sim$ 16%. Assuming a Gaussian distribution and 8% to be the 3-σ level, then the radiosonde analysis indicates the tropospheric doppler error has a σ of $\sim$ 2.8% of the nominal value.

An additional influence was introduced into the second series of reductions. The doppler observables were weighted (Fig. 9) by the DPODP weighting function (Ref. 2).

$$\sigma_{obs}\,(a\,priori) = 0.1\,\text{mm/s}$$

($\sim$2 times larger than the deduced 1 σ from O − C high-frequency noise)

$$\sigma_{obs}\,(\text{DPODP}) = \sigma_{obs}\,(a\,priori)\left[1 + \frac{18}{(1+\gamma^2)}\right]$$

where γ = elevation in degrees.

$$\omega t_{obs}\,(\text{DPODP}) = \frac{1}{\sigma^2_{obs}\,(\text{DPODP})}$$

where ωt = weight applied to observable.

Table 4 contains the DPODP estimates of N_{11}, pass by pass. From the scatter of N_{11} relative to the nominal value of N_{11}, 240 N units, and the "formal" solution σs, it is apparent that the *a priori* σ of N_{11} is too conservative. It is of value to note the characteristics of the pass-by-pass solutions for DSS 11 spin-axis distance and longitude. The spin-axis distance $r_{s_{11}}$ solutions that result when N_{11} is used to exercise a constrained—yet variable scaling of the

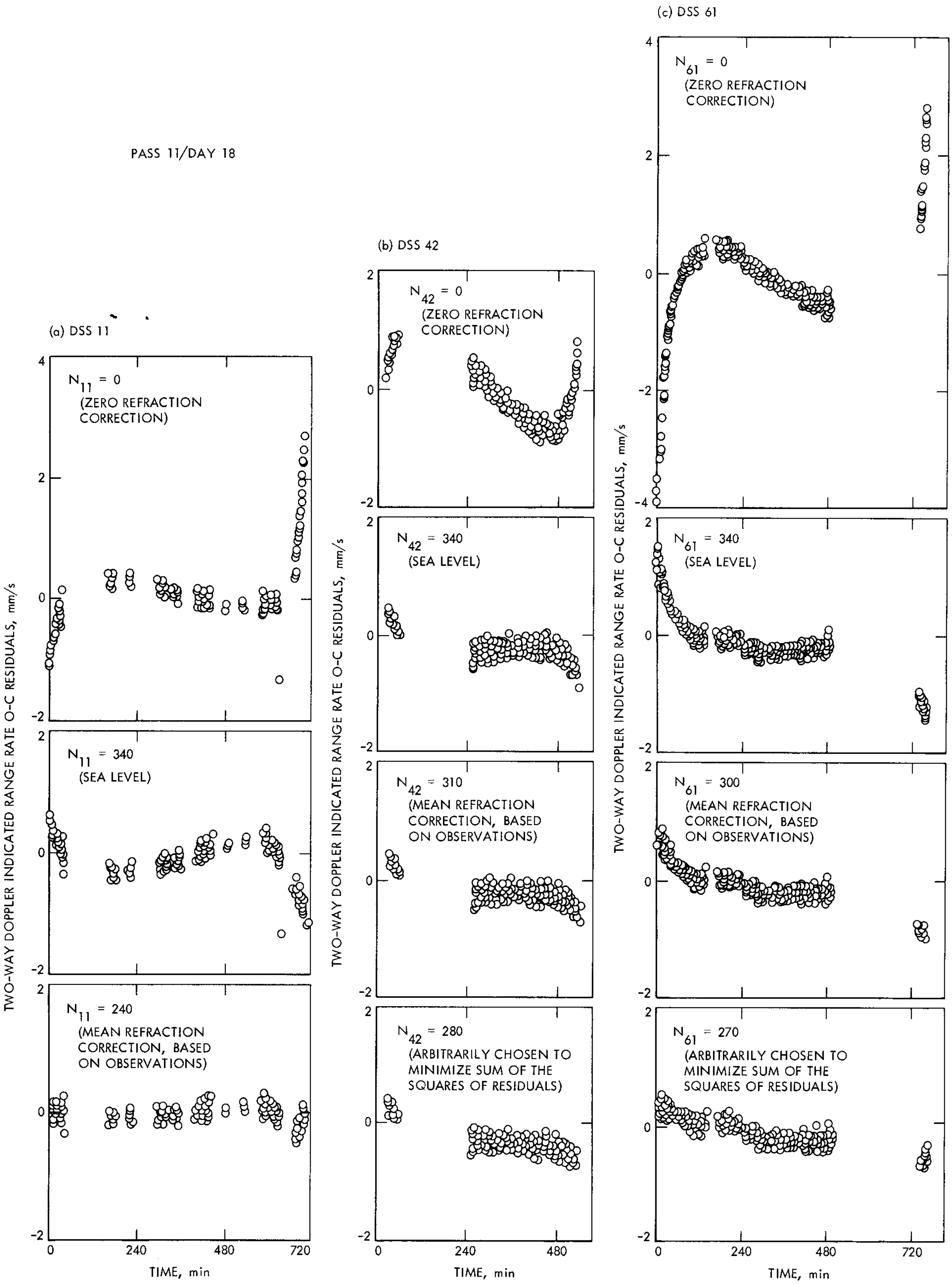

Fig. 6. Sensitivity of O — C residual profiles to the tropospheric variable *N*

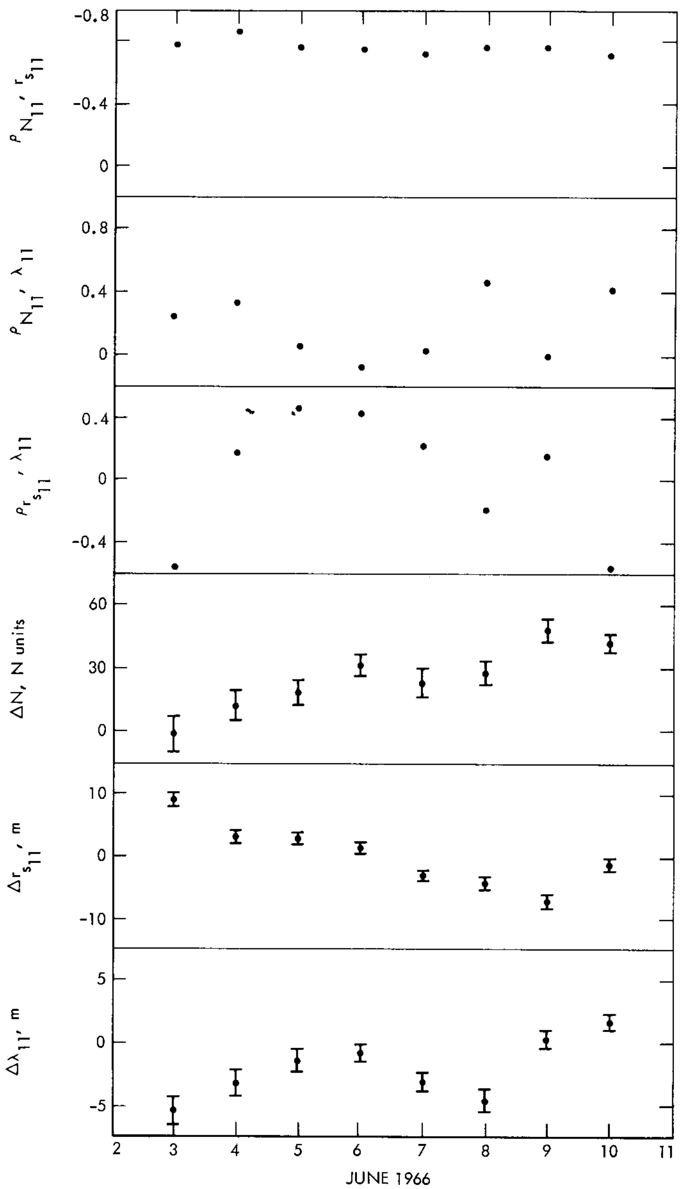

Fig. 7. DSS 11—*Surveyor VI* tracking data fits (individual passes)

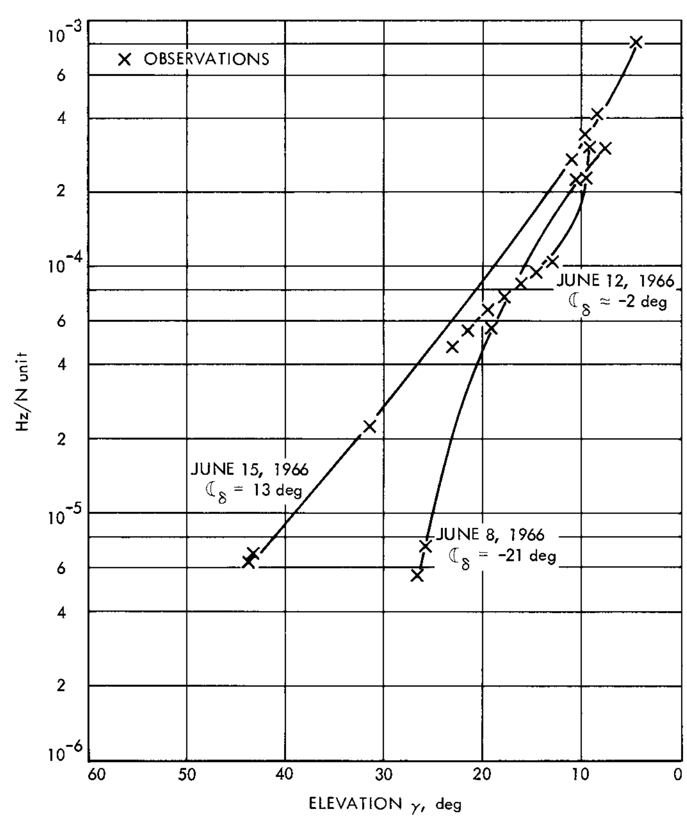

Fig. 8. Partials of doppler with respect to N_{11}

Table 4. DSS 11 refractivity scaler estimates[a]

Surveyor	Average N_{11}	Pass																					
		3		4		5		6		7		8		9		10		11		12		13	
		N_{11}	σ	N_{11}	σ	N_{11}	σ	N_{11}	σ	N_{11}	σ	N_{11}	σ	N_{11}	σ	N_{11}	σ	N_{11}	σ	N_{11}	σ	N_{11}	σ
I	251	244	3.7	246	3.6	246	3.5	253	3.1	246	3.6	261	2.8	250	3.6	265	2.4	—	—	—	—	—	—
III	—	—	—	—	—	—	—	—	—	—	—	—	—	—	—	—	—	—	—	—	—	—	—
V	231	234	3.6	233	3.8	—	—	—	—	230	3.4	225	3.0	236	3.8	239	4.0	220	2.9	234	3.2	—	—
VI	233	237	3.8	225	3.0	231	3.5	220	2.8	231	3.6	234	3.7	—	—	240	4.0	240	3.9	240	4.0	—	—
VII	229	—	—	—	—	—	—	—	—	232	3.5	226	2.9	231	3.6	222	2.6	225	2.7	237	4.0	—	—

[a]Conditions imposed on fit:
(1) the doppler was off-weighted as a function of elevation; (2) the refractivity scaler *a priori* σ was 4 N units.

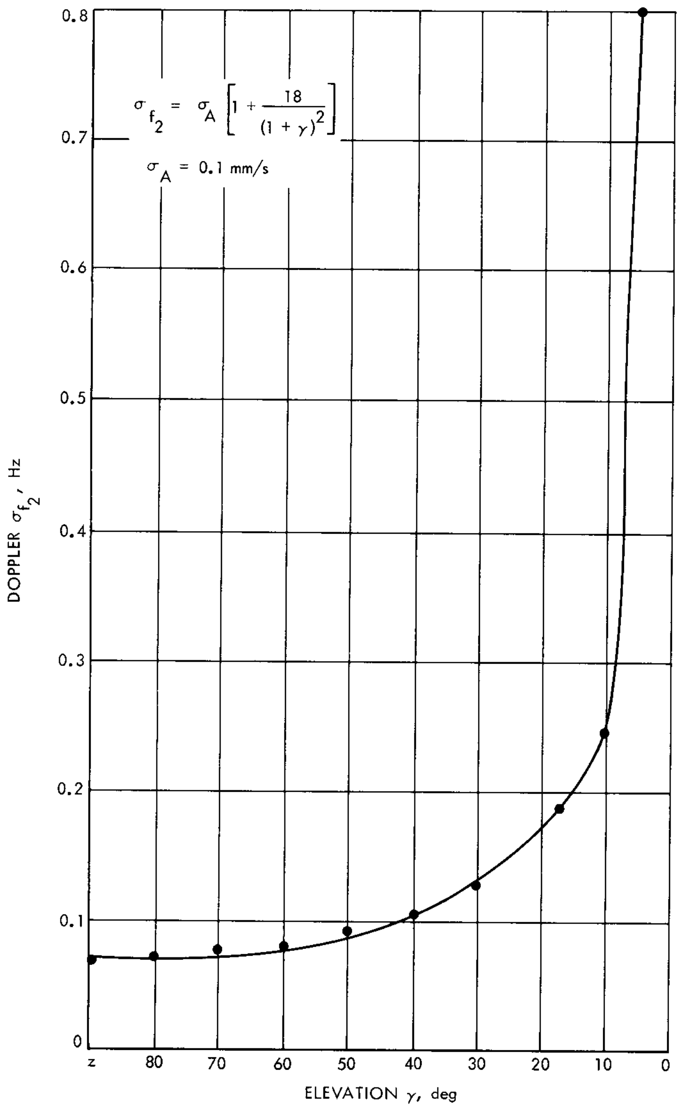

Fig. 9. DPODP doppler observable weighting as a function of elevation

tropospheric function—have less scatter than the analogous set of r_s solutions in which N_{11} was held to be a constant (Fig. 10). The sensitivity of r_s to the scaling of the tropospheric corrections (variation in N) is shown in Fig. 10. The DSS longitude solutions are only slightly influenced by the inclusion of N_{11} as a parameter.

VI. Estimates of N_{11} (Pass by Pass)

The first two series of data fits have provided an understanding of parameter cross-correlations and some understanding of the positive value of inclusion of N_{11} into the solution parameter list.

This series presents data fits to the N_{11} parameter. From these estimates of N_{11}, formal statistics are generated which reveal the strength of the doppler, pass by pass, to solve for N_{11}. The solutions are presented graphically (Fig. 11). It is anticipated that the solutions will change once ionospheric charged particle calibrations are applied to the doppler.

The formal statistics do not reflect the imperfection of the modeler's universe; DSS location errors, polar motion errors, UT1 errors, etc., are assumed non-existent. Thus, the statistics are optimistic and represent some abstract ideal. [This is the reason for weighting the doppler observable with the unit weight of 0.1 mm/s (~2 times the observed high-frequency noise associated with the O − C residuals). Admittedly, the factor of ~2 is subjective.]

The scatter of the N_{11} estimates is ~16–25%. This total percentage variation is the sum of the percentage variation of the estimates over any given lunation (8–10%) and the percentage change from lunation to lunation

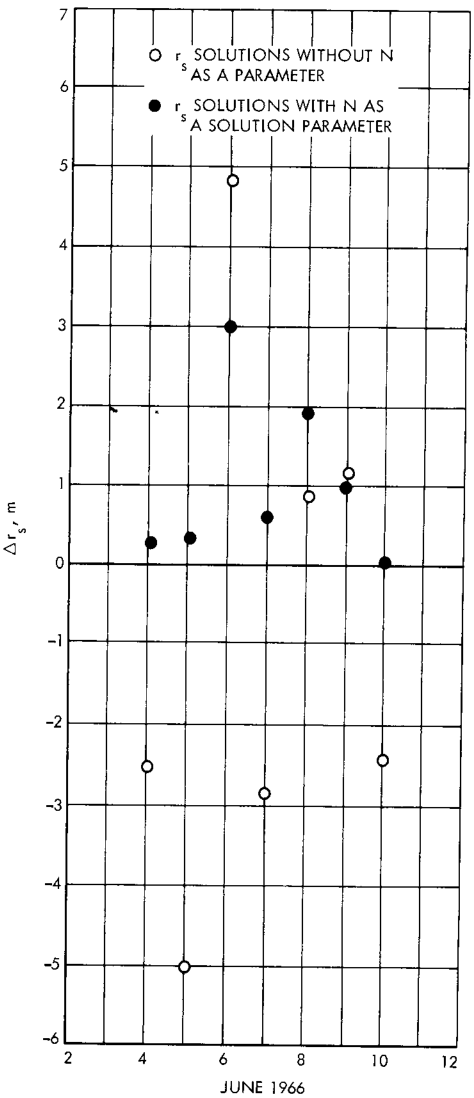

Fig. 10. Surveyor I–DSS 11 r_s solutions

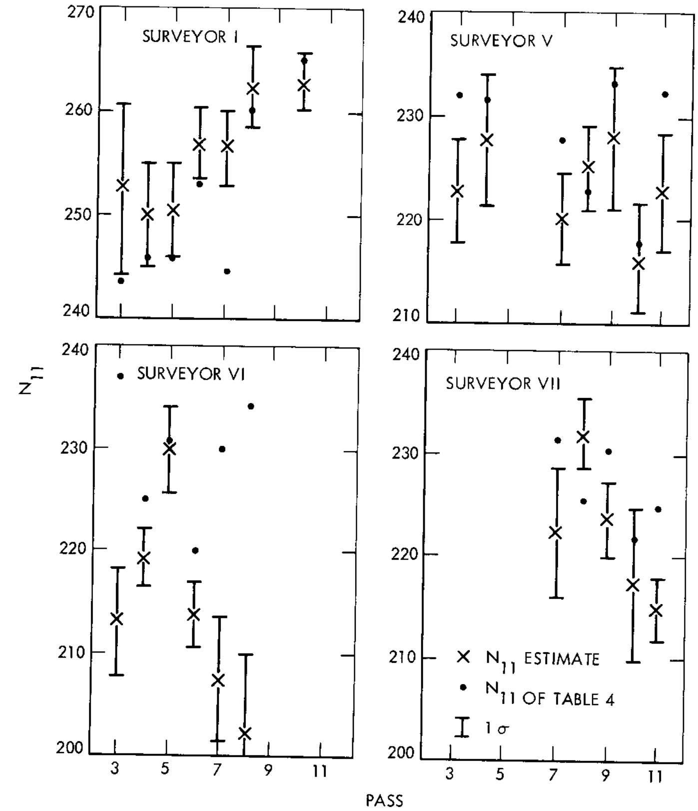

Fig. 11. N_{11} estimates

(~8–15%). Thus, the 16–25% change is the extreme variation.

Radiosonde analysis shows zenith–range errors (tropospheric-induced) to undergo variations of ~8% (Ref. 9). Additionally, the variability of the refractivity versus altitude profile from day to day produces errors of ~8% when a mapping function is used to scale the zenith–range error to 5-deg elevation (L. F. Miller, V. J. Ondrasik, and C. C. Chao in the previous article). Thus, radiosonde analysis shows a 16% variation (in the extreme) for observations taken at 5-deg elevation.

It is the doppler data taken at the very low elevations (5–10 deg) which contain the most information concerning the solution for N_{11}. It is not uncommon for the partials of the doppler observable (CC3) with respect to N_{11} to increase an order of magnitude from 20- to 5-deg elevation. The $\partial CC3/\partial N_{11}$ falls off very fast with increasing elevation (Fig. 8). Yet, the high-elevation data do have some influence, and, as a consequence the tracking data estimates N_{11} ideally should have less variation than the radiosonde determinations presented above. It is hoped that once ionospheric effects are included the scatter will diminish. Additionally, the cross-correlations unveiled by the second series of fits indicate that DSS location errors will influence N_{11} estimates as a function of the pass data acquisition pattern.

The seasonal variations of the magnitude of the tropospheric influence shown by one year (1967) of radiosonde data (Ref. 9) cannot be seen in the empirical data fits to N_{11} because only two spacecraft (*Surveyors V* and *VI*) functioned during the radiosonde data interval that were tracked at DSS 11. If the radiosonde measures of 1967 were applied to adjacent years, just to deduce the seasonal trends, the doppler fits would not agree.

The response of the O − C residuals to the introduction of N_{11} as a parameter can most easily be shown by a comparison of the second moments μ_2 of the residuals after the fits. The μ_2 associated with a typical pass are reduced by ~75–80% when N_{11} is estimated. Some elevation-dependent O − C variations are still characteristic of the fits. This is in part due to the ionospheric influences. Figure 12 provides a typical set of O − C residuals after the fit in which N_{11} was and was not estimated.

Elevation-dependent O − C signatures occur in the O − C residuals at elevations as high as 25 deg. When N_{11} is estimated, the quality of the fit is extended to 15-deg elevation, that is, the O − C "diurnal" signature does not appear above 15-deg elevation.

When an entire lunation is fitted solving for DSS spin-axis distance and longitude, with and without N as an accompanying parameter, the quality of the fit is extended very little over the elevation range although the magnitude of the O − C variations are reduced ~18%. Table 5 presents the μ_2 of the lunation fits in which N was and was not estimated.

Table 5. μ_2 associated with lunation fits

Surveyor	Estimated parameters		Decrease, %
	N_{11}, $r_{s_{11}}$, λ_{11}	$r_{s_{11}}$, λ_{11}	
I	0.0490	0.0591	17.1
V	0.0449	0.0564	20.2
VI	0.0439	0.0502	12.6
VII	0.0391	0.0489	19.9

VII. Conclusions

In conclusion, the following observations are summarized:

(1) *Mariner, Lunar Orbiter,* and *Surveyor* doppler data reveal elevation-dependent O − C residuals which are related to tropospheric refraction effects. (Ionospheric influences are yet to be calibrated.)

(2) The employment of *Surveyor* doppler data to estimate refractivity effects removes all terrestrial media type structures from O − C sets above 15-deg elevation when fit on a pass-by-pass basis. The resultant μ_2 of the fits are reduced ~80%.

(3) If no effort is made to estimate refraction effects, the O − C set exhibits media type variation at ~25-deg elevation, and the amplitude of O − C variations at low elevations (below 10 deg) can be as large as millimeters per second.

(4) Cross-correlations are quite large between the refractivity parameter and some of the parameters on the parameter list. Cross-correlations between N and the parameter list vary according to spacecraft declination and the data acquisition pattern for a pass.

(5) The cross-correlation between the refractivity parameter and the distance off the spin axis for a given station is large enough to preclude simultaneous solution for both. External information concerning the value of one or the other parameter must be available.

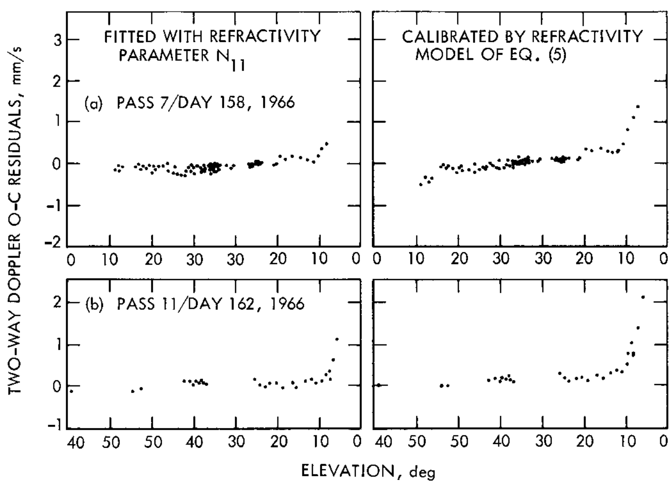

Fig. 12. Refractivity parameter influence on Surveyor I–DSS 11 O − C residuals

References

1. Hamilton, T. W., and Melbourne, W. G., "Information Content of a Single Pass of Doppler Data from a Distant Spacecraft," in *The Deep Space Network*, Space Programs Summary 37-39, Vol. III, pp. 18–23. Jet Propulsion Laboratory, Pasadena, Calif., May 31, 1966.

2. Flynn, J. A., et al., *Double Precision Orbit Determination Program, Vol. V, Links Observ., Regres., Parts,* Report 900–298. Jet Propulsion Laboratory, Pasadena, Calif., Sep. 26, 1969.

3. Warner, M. R., and Nead, M. W., *SPODP–Single Precision Orbit Determination Program,* Technical Memorandum 33-204. Jet Propulsion Laboratory, Pasadena, Calif., Feb. 15, 1965.

4. Liu, A., "Recent Changes to the Tropospheric Refraction Model Used in the Reduction of Radio Tracking Data From Deep Space Probes," in *The Deep Space Network,* Space Programs Summary 37-50, Vol. II, pp. 93–97. Jet Propulsion Laboratory, Pasadena, Calif., Mar. 31, 1968.

5. Cary, C., "Spacecraft on the Lunar Surface, Part I–Range-Rate Tracking," in *The Deep Space Network,* Space Programs Summary 37-47, Vol. II, pp. 4–11. Jet Propulsion Laboratory, Pasadena, Calif., Sep. 30, 1967.

6. Winn, F. B., "Preliminary *Surveyor VI* Postlanded Tracking Data Analysis," in *The Deep Space Network,* Space Programs Summary 37-50, Vol. II, pp. 110–125. Jet Propulsion Laboratory, Pasadena, Calif., Mar. 31, 1968.

7. Winn, F. B., "Post-Lunar Touchdown Tracking Data Analysis," in *The Deep Space Network,* Space Programs Summary 37-51, Vol. II, pp. 42–50. Jet Propulsion Laboratory, Pasadena, Calif., May 31, 1968.

8. Brouwer, D., and Clemence, G. M., *Methods of Celestial Mechanics.* Academic Press, New York, 1961.

9. Ondrasik, V. J., and Thuleen, K. L., "Variations in Zenith Tropospheric Range Effect Computed From Radiosonde Balloon Data," in *The Deep Space Network,* Space Programs Summary 37-65, Vol. II, pp. 25–35. Jet Propulsion Laboratory, Pasadena, Calif., Sep. 30, 1970.